Tuning of the Electronic Characteristics of ZnO Nanowire Field Effect Transistors by Proton Irradiation

Woong-Ki Hong,[†] Gunho Jo,[†] Jung Inn Sohn,[‡] Woojin Park,[†] Minhyeok Choe,[†] Gunuk Wang,[†] Yung Ho Kahng,[†] Mark E. Welland,[‡] and Takhee Lee[†,*]

[†]Department of Materials Science and Engineering, Gwangju Institute of Science and Technology, Gwangju 500-712, Korea, and [‡]Nanoscience Centre, University of Cambridge, Cambridge CB3 0FF, United Kingdom

ABSTRACT We demonstrated a controllable tuning of the electronic characteristics of ZnO nanowire field effect transistors (FETs) using a high-energy proton beam. After a short proton irradiation time, the threshold voltage shifted to the negative gate bias direction with an increase in the electrical conductance, whereas the threshold voltage shifted to the positive gate bias direction with a decrease in the electrical conductance after a long proton irradiation time. The electrical characteristics of two different types of ZnO nanowires FET device structures in which the ZnO nanowires are placed on the substrate or suspended above the substrate and photoluminescence (PL) studies of the ZnO nanowires provide substantial evidence that the experimental observations result from the irradiation-induced charges in the bulk SiO_2 and at the SiO_2/ZnO nanowire interface, which can be explained by a surface-band-bending model in terms of gate electric field modulation. Our study on the proton-irradiation-mediated functionalization can be potentially interesting not only for understanding the proton irradiation effects on nanoscale devices, but also for creating the property-tailored nanoscale devices.

KEYWORDS: semiconductor nanowires · ZnO nanowires · electronic transport · field effect transistors · proton irradiation

Nanomaterial-based field effect transistors (FETs) with novel functionalities have attracted great interest as basic elements for nanoscale device applications such as sensing devices, memory devices, and logic circuits.[1−4] Accordingly, to date, there have been considerable efforts to produce and improve diverse functionalities by surface modification,[5,6] band structure engineering,[7−9] gate structure engineering,[10,11] polarity control,[12−14] doping control,[15] and irradiation-induced modification.[16−22]

In particular, many irradiation studies of various nanomaterials with energetic particles, such as electrons or ions, have demonstrated that irradiation can have beneficial effects providing devices with desired functions; it may be used to tailor the structural, mechanical, electronic, and even magnetic properties of nanomaterials.[16−22] Thus, the irradiation of nanomaterials, as a useful tool for engineering nanosystems and tailoring their properties, can provide potentially useful ways to create property-tailored and functionalized devices based on nanomaterials for applications in nanoelectronics, energy, and nanobiotechnology.[16−22] Recent related works have shown that the electrical properties of carbon nanotubes (CNTs) or nanoscale devices can be tuned by irradiation.[21−23] For example, metal-to-insulator or metal-to-semiconductor transitions in single-walled CNTs by electron beam irradiation have been reported.[21,22] We have also demonstrated that hybrid complementary logic circuits, which comprise n-type ZnO nanowire FETs and p-type single-walled CNT FETs, can be successfully realized by adjustment of the threshold voltage through proton beam irradiation.[23] As for realizing nanoscale logic devices with desired functions, one of the major challenges is controlling the operation voltage in nanoscale FETs.[24,25] To this end, proton-irradiation-mediated engineering has been introduced in nanowire-based FETs.[23] To our knowledge, no such beneficial functionalization has been reported for nanowire-based transistors. Therefore, it will be particularly useful to understand and develop proton-irradiation-mediated engineering in nanoscale devices for achieving desired functions and practical applications.

In this study, we have fabricated and characterized two types of ZnO nanowire FET device structures in which the nanowires are placed on the substrate or suspended above the substrate, both in a conventional back-gate FET configuration, which provides effective platforms to address the controllable tuning of the electronic properties in nanoscale devices by surface band engineering through the proton

*Address correspondence to tlee@gist.ac.kr.

Received for review October 15, 2009 and accepted January 22, 2010.

Published online January 29, 2010.
10.1021/nn9014246

irradiation. We have observed that the threshold voltage shift and the electrical conductance modulation of the on-substrate-type FET devices are attributed to irradiation-induced positively charged oxide-trapped holes (or positive oxide traps) or negatively charged interface states (or negative interface traps), which is confirmed by the characteristics of the suspended-type FET devices and PL measurements of the ZnO nanowires. In addition, we describe the proton irradiation effects on the ZnO nanowire FETs in terms of the electric field based on a surface-band-bending model. An understanding of the proton irradiation effects on nanoscale devices is likely to open up a new avenue for harnessing irradiation for nanomaterials and proton-beam-mediated engineering.

RESULTS AND DISCUSSION

Two types of FET devices, an "on-substrate" type where nanowires are placed on the substrate and a "suspended" type where nanowires are suspended above the substrate, were fabricated using single-crystal ZnO nanowires grown by a vapor transport method (see Experimental Methods for detailed device fabrication). Note that these nanowire FET devices are coated by poly(methyl methacrylate) (PMMA) to reduce the hysteresis caused by water or gas molecules in the ZnO nanowire FETs (see also Figures S1 and S2 in the Supporting Information).[26] The proton irradiation of the on-substrate type ZnO nanowire FET devices is schematically illustrated in Figure 1a, which also shows a scanning electron microscopy (SEM) image of a fabricated device. The electrical characteristics of the on-substrate-type FETs are summarized in Figures 1 and 2. Figure 1 shows the representative data of the output characteristics (source-drain current *versus* voltage, $I_{DS}-V_{DS}$) and transfer characteristics (source-drain current *versus* gate voltage, $I_{DS}-V_G$) before and after proton irradiation with fluences of 10^{10} cm^{-2} (Figure 1b) and 10^{12} cm^{-2} (Figure 1c), respectively (see also Figure S3 in the Supporting Information for a fluence of 10^{11} cm^{-2}). The $I_{DS}-V_{DS}$ curves have well-defined linear regimes at low biases and saturation regimes at high biases both before and after proton irradiation, indicating typical pinch-off characteristics of n-type semiconductor FETs.[27,28] A major finding in the $I_{DS}-V_{DS}$ curves is that the electrical conductance increased after a short irradiation time ($\Phi = 10^{10}$ cm^{-2} corresponding to an irradiation time of 60 s) under the same applied gate bias conditions, whereas after long irradiation times ($\Phi = 10^{11}$ cm^{-2} corresponding to 600 s and $\Phi = 10^{12}$ cm^{-2} corresponding to 6000 s), the electrical conductance decreased (see also Figure 2b). Moreover, the $I_{DS}-V_G$ curves reveal that the on-substrate-type FET exhibits a negative threshold voltage shift after a short irradiation time, whereas the device displays a positive threshold voltage shift after a long irradiation time (see also Figure 2a and Figure S3b in the Supporting Information). To allow for statistical descriptions of the threshold voltage shift and the electrical conductance modulation of these on-substrate-type FETs after proton irradiation, a total of 54 nanowire FET devices were fabricated and systematically characterized: 21 FETs, 17 FETs, and 16 FETs at fluences of 10^{10} cm^{-2} (60 s), 10^{11} cm^{-2} (600 s), and 10^{12} cm^{-2} (6000 s), respectively. Figure 2a shows a plot of the threshold voltage as a function of proton irradiation time. The threshold voltages of the on-substrate-type FETs were found to be -0.97 ± 0.59, 2.27 ± 0.75, and 4.37 ± 0.98 V for irradiation times of 60, 600, and 6000 s, respectively. Importantly, the threshold voltage shifted to the negative gate bias direction after a short irradiation time, and to the positive gate bias direction after a long irradiation time.

It is well-known that ionizing irradiation of high-energy electrons or protons can generate electron−hole pairs in SiO_2, resulting in irradiation-induced charges.[29−31] The inset of Figure 2a presents a schematic energy band diagram of an on-substrate-type FET structure, illustrating the generation of electron−hole pairs by proton irradiation. When a ZnO nanowire FET is exposed to a high-energy proton beam, electron−hole pairs are created in the SiO_2 layer, which is the layer most sensitive to ionizing irradiation. Immediately after electron−hole pairs are generated, most of the electrons can be rapidly (within picoseconds) swept out of the bulk SiO_2 layer due to their high mobility.[29−31] As a result, some of the irradiation-induced holes may be trapped at the localized trap sites in the bulk SiO_2 layer, leading to the positive oxide-trapped charges (or positive oxide traps, Q_{ot}). In addition, some fraction of the irradiation-induced holes and protons in the SiO_2 can transport to the SiO_2/ZnO nanowire interface and then interact with the ZnO surface, leading to the formation of interface states (or interface traps, D_{it}), which are negatively charged as electron trap centers for n-channel transistors.[29−31] The generation of such charges can play a key role in the controllable tuning of the electrical properties of ZnO nanowires. For instance, negatively charged molecules adsorbed at the ZnO surface accept electrons, leading to surface depletion and a reduction in conductivity, whereas positively charged molecules act as electron donors, leading to an increase in the carrier concentration and conductivity in n-type ZnO nanowires.[32] Similarly, for the on-substrate-type FETs, the positive oxide traps and negative interface traps, which are induced by proton irradiation, have a significant influence on the surface depletion and carrier concentration in the ZnO nanowire channel, which is responsible for the tuning of the operation voltage as well as the modulation of the electrical conductance. Specifically, the positive oxide traps in the bulk SiO_2 layer act as an enhancement of the gate electric field, resulting in an increased carrier concentration and a negative threshold voltage shift. On the

other hand, the negative interface traps increase the surface depletion region, resulting in a reduction of carrier concentration and a positive threshold voltage shift. In particular, since the irradiation-induced interface states occur on a time scale much slower than that of oxide traps in the bulk SiO_2 layer, the total threshold voltage shift is the sum of the threshold voltage shifts due to oxide traps and interface traps for a gate-oxide transistor.[29−31] Therefore, the observed threshold voltage shift of on-substrate-type FETs after proton irradiation can be explained by the combination effects of oxide traps and interface states.[27−31]

In accordance with the threshold voltage shift, Figure 2b shows the normalized conductance as a function of proton irradiation time. Here, the normalized conductance is the ratio of the conductance after proton irradiation to that before proton irradiation. The electrical conductance increased after a short irradiation time but decreased after long irradiation times, indicating a modulation of the gate electric field-induced carrier concentration of the nanowire channel.[33] Figure 2c and 2d show contour plots of the transconductance ($g_m = dI_{DS}/dV_G$), which were obtained from $I_{DS}-V_G$ curves measured for V_{DS} in the range of 0.02−1 V, as a function of the gate electric field (V_G-V_{th}) and source-drain electric field (V_{DS}) before and after proton radiation at fluences of 10^{10} and 10^{12} cm^{-2}, respectively (see also Figure S3c in the Supporting Information). The transconductance increased with V_{DS} both before and after proton irradiation. However, under the same applied gate field, the transconductance was higher after a short irradiation time but lower after a long irradiation time, in comparison to the case before irradiation. Here, we found that the gate field effect depends sensitively on the irradiation-induced charges and the gate electric field modulation, which will be explained later using a surface-band-bending model.

To provide substantial evidence that the observed threshold voltage shift in the on-substrate-type FETs can really be attributed to two different types of irradiation-induced charges, and in particular to unambiguously explain the effect of irradiation-induced interface states at the SiO_2/ZnO nanowire interface, we fabricated ZnO nanowire FET devices in a suspended-type structure, which has no effect by the interface states at the SiO_2/ZnO nanowire interface. A total of 17 suspended-type devices were fabricated and characterized before and after proton irradiation: 6 FETs, 5 FETs, and 6 FETs at fluences of 10^{10}, 10^{11}, and 10^{12} cm^{-2}, respectively. Figure 3a displays the detailed process of fabricating suspended-type nanowire FET devices. First, droplets of the nanowire suspension

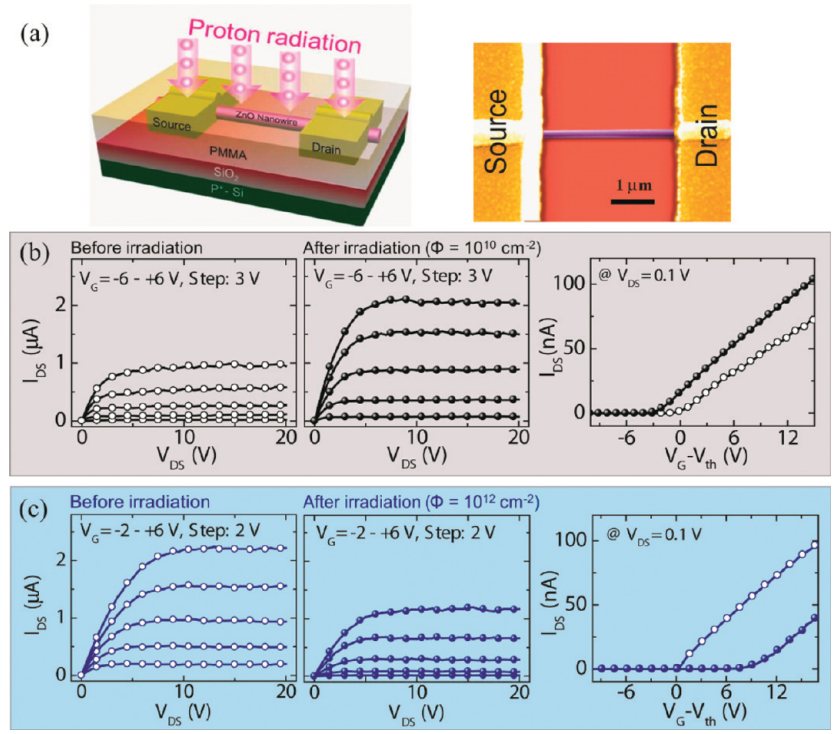

Figure 1. (a) Schematic illustrating proton irradiation of ZnO nanowire FET devices. A SEM image of an on-substrate-type ZnO nanowire FET device is shown. (b, c) Electrical characteristics before (open circles) and after (filled circles) proton irradiation at an energy of 10 MeV with fluences of (b) 10^{10} cm^{-2} (corresponding to an irradiation time of 60 s) and (c) 10^{12} cm^{-2} (corresponding to an irradiation time of 6000 s).

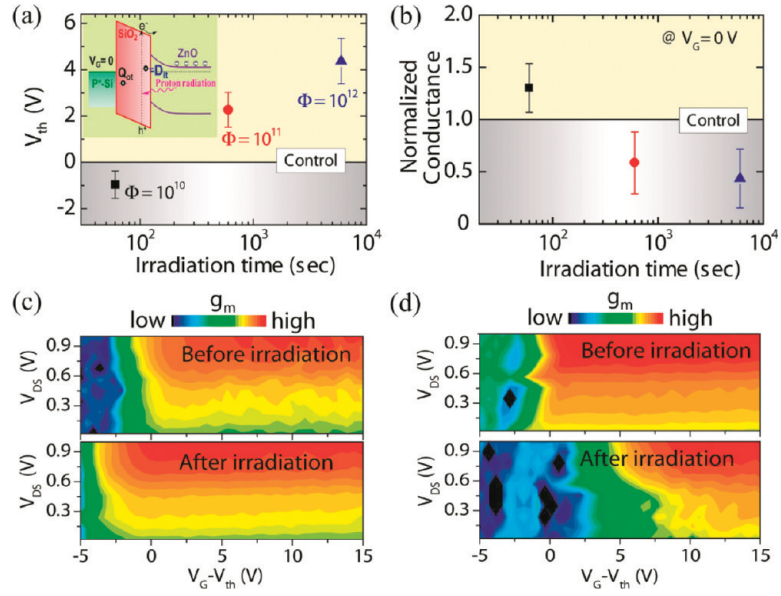

Figure 2. (a) Threshold voltage shift and (b) normalized conductance of the on-substrate-type ZnO nanowire FETs as a function of proton irradiation time (60, 600, and 6000 s). The inset in (a) shows a schematic energy band diagram of the on-substrate-type FET device structure, illustrating proton-irradiation-induced electron−hole pairs. (c, d) Contour plots of transconductance (g_m) as a function of the gate electric field (V_G-V_{th}) and source-drain electric field (V_{DS}) before and after irradiation at fluences of (c) 10^{10} cm^{-2} (60 s) and (d) 10^{12} cm^{-2} (6000 s).

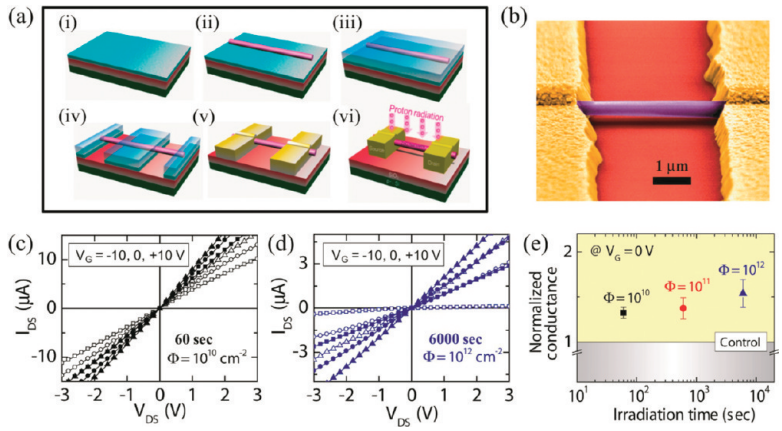

Figure 3. (a) Schematic views of the fabrication steps of a suspended-type ZnO nanowire FET device (see text for details). (b) A SEM image of a single ZnO nanowire suspended above the substrate. (c, d) $I_{DS}-V_{DS}$ characteristics with various gate bias voltages (V_G = −10, 0, +10 V) before (open symbols) and after (filled symbols) proton irradiation at an energy of 10 MeV with fluences of (c) 10^{10} cm^{-2} (60 s) and (d) 10^{12} cm^{-2} (6000 s). (e) Normalized conductance of suspended-type nanowire FETs as a function of proton irradiation time.

were spin-coated onto a very thin photoresist-coated Si substrate with a 300 nm-thick SiO_2 layer (steps i and ii). Lithographic patterning was used to open windows in the photoresist over the source (S) and drain (D) electrode contact regions on the nanowire (steps iii and iv). Electron-beam evaporation of Ti (200 nm)/Au (200 nm) followed by the lift-off process was used to complete the source and drain contacts, and a ~3 μm channel was defined by the electrodes (step v). Then, the fabricated suspended-type devices were irradiated by a proton beam (step vi). A SEM image of a fabricated suspended-type device is shown in Figure 3b. The electrical properties of the suspended-type devices before and after proton irradiation are summarized in Figure 3c−e (see also Figure S4 in the Supporting Information for a fluence of 10^{11} cm^{-2}). All of the $I_{DS}-V_{DS}$ curves before and after irradiation show almost linear characteristics, indicating a good ohmic contact with a very low Schottky barrier height.[34] Notably, the suspended-type FET devices have a relatively weaker gating effect in the gate voltage range between −10 and +10 V due to the suspended geometry. Interestingly, unlike the case for on-substrate-type devices (Figure 1b,c), the current−voltage characteristics ($I_{DS}-V_{DS}$) at various gate biases in the suspended-type devices (Figure 3c,d) show an increase in the electrical conductance due to proton irradiation effects for both short and long irradiation times (see also Figure S4 in the Supporting Information). The statistical data in Figure 3e clearly show an increase in the normalized electrical conductance for all of the fabricated suspended-type devices after proton irradiation. As discussed earlier, this observation can be explained by the existence of only irradiation-induced positive oxide traps without the interface-state effect, resulting in an enhancement of the gate electric field in the suspended-type device structure. In other words, the increased conductance at the same applied gate bias after irradiation exhibits an increased carrier concentration induced by an enhancement of the gate electric field due to positive oxide traps in this type of device structure.

To elucidate the proton irradiation effects on ZnO nanowire FET devices, we further investigated whether the ZnO nanowire itself was affected or not by the proton irradiation using microphotoluminescence (μPL) and temperature-dependent PL measurements. The optical properties of the ZnO nanowires with irradiation time (fluence) are presented in Figure 4. In general, the PL emissions of the ZnO nanowires consist of an ultraviolet (UV) emission band with a peak position between 375 and 380 nm and a deep level (DL) emission (or defect emission) in the broad visible range, which is attributed to surface defects.[35] Figure 4a shows the integrated PL intensity ratio (UV emission intensity to defect emission intensity, I_{UV}/I_{DL}), which is obtained from the PL spectra (the inset of Figure 4a), as a function of proton irradiation time. Interestingly, no significant change was observed in the PL intensity ratios, indicating the radiation hardness of the ZnO nanowires.[36−39] Figure 4b shows the temperature-dependent PL spectra of ZnO nanowires in the temperature range of 10−300 K. It is well-known that the PL spectra of ZnO nanostructures is commonly attributed to the direct recombination of excitons through an exciton−exciton scattering.[40] Here, we have found that the PL characteristics originate mainly from the recombination of free exciton (FX) and donor bound exciton (D^0X) since a free exciton (FX), a neutral-donor-bound exciton (D^0X), and their longitudinal optical (LO) phonon replicas, which are located at the same energy positions at low temperature, are clearly seen in Figure 4b. The LO-phonon replicas of FX and D^0X are labeled FX-1LO (F1), FX-2LO (F2), FX-3LO (F3), D^0X-1LO (D1), D^0X-2LO (D2), and D^0X-3LO (D3). The FX and D^0X peaks are located at ~3.375 and ~3.354 eV, respectively. Their LO-phonon replicas are observed with a separation of ~72 meV, which corresponds to the LO-phonon energy of ZnO.[40,41] These pronounced replicas originate from the strong exciton−phonon coupling effect due to the high ionicity and polarity of ZnO.[42] The exciton emission shifts to lower energy with increasing temperature due to thermal activation of carriers,[42,43] and the FX and its LO-phonon replicas become stronger in intensity relative to the D^0X-related peak. In addition, as temperature increases, the D^0X-related emissions decrease more rapidly than the FX-related emissions due to thermal dissociation of the

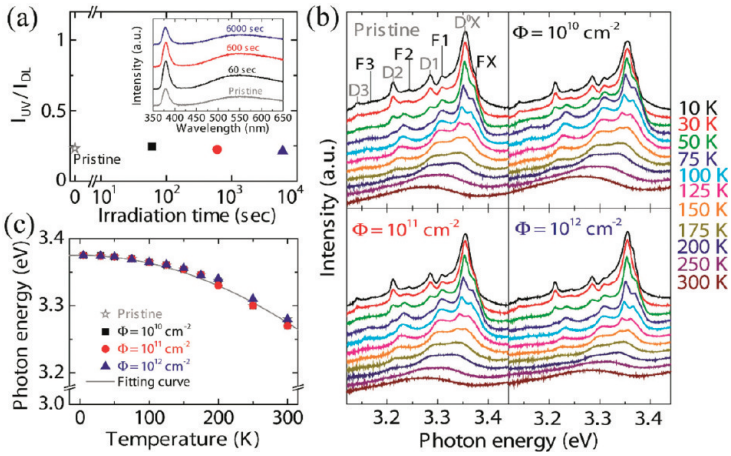

Figure 4. (a) Integrated photoluminescence (PL) intensity ratios (I_{UV}/I_{DL}) as a function of the proton iradiation time. The inset shows the PL spectra of as-grown (pristine) and proton-irradiated ZnO nanowires. (b) Temperature-dependent PL spectra, showing the excitons and their LO-phonon replicas for the pristine and proton-irradiated ZnO nanowires. (c) Temperature dependence of FX peak position. The solid line is a fitting curve of the experimental data by Varshni's formula.

donor-bound-related excitons, and thus the FX-related emissions remain at room temperature. All these results indicate that for the pristine and proton-irradiated ZnO nanowires, D^0X-related transitions are dominant at low temperature, whereas FX-related transitions are dominant at high temperature. Figure 4c shows the temperature-dependent FX peak positions in the temperature range of 10−300 K for the pristine and proton-irradiated ZnO nanowires. The temperature dependence of the FX transition energy can be expressed by Varshni's empirical formula[42]

$$E(T) = E(0) - \frac{\alpha T^2}{T + \beta} \quad (1)$$

where α and β are constants and $E(0)$ is an exciton energy at $T = 0$ K. The fit is plotted as a solid line through the data points in Figure 4c. It is found that the empirical Varshni's expression adequately predicts the positions of the FX peaks as a function of temperature. The fitting parameters $E(0)$, α, and β are 3.375 eV, 0.00685 eV/K^{-1}, and 5840 K for both the pristine and proton-irradiated ZnO nanowires. It can be clearly seen that the peak positions of FX for the proton-irradiated ZnO nanowires do not change with respect to those for the pristine ZnO nanowires, indicative of irradiation hardness of the ZnO nanowires themselves.[36−39] Here, we have found that the proton irradiation did not influence the structures of the ZnO nanowires. Therefore, the proton irradiation effects on the ZnO nanowire FET devices (Figures 1−3) are due to the irradiation-induced charges in the bulk SiO_2 layer and at the SiO_2/ZnO nanowire interface, but not by the ZnO nanowires themselves.

Here, the experimental observations of the proton beam irradiation effects on the two types of device structures studied are explicitly explained using a surface-band-bending model, as shown in Figure 5. Figure 5 panels a and b show the schematics and the corresponding equilibrium energy band diagrams at $V_G = 0$ V before and after proton irradiation of the on-substrate-type and suspended-type ZnO nanowire FET devices, respectively. For the on-substrate-type FET device after a short irradiation time (Figure 5a, middle), the electronic conduction (E_C) and valence (E_V) bands of ZnO show surface-band-bending with a smaller surface depletion width (W_{d1}) and a relatively lower surface barrier potential (φ_{S1}) at the SiO_2/ZnO nanowire interface, resulting from an enhancement of the gate electric field due to the positive oxide traps (Q_{ot}) in the bulk SiO_2. The formation of such a constructive electric field causes the threshold voltage to shift toward the negative gate bias direction and results in an increase in the electrical conductance under the same applied gate bias. Conversely, the electronic bands observed after a long irradiation time (Figure 5a, bottom) show surface-band-bending with a relatively larger surface depletion width (W_{d2}) and higher surface barrier potential (φ_{S2}), resulting from the formation of a destructive electric field due to the negative interface traps (D_{it}). In other words, for the case of long irradiation times, a strong electric field (φ_{dep}) exists in an extended surface depletion region due to increased surface-band-bending by the interface states.[44,45] The effective gate electric field experienced by the carriers in the channel, taking into consideration the cylindrical nanowire channel geometry, can be estimated using the following equations:[28]

$$\xi_{eff} = \frac{1}{\varepsilon_{ZnO}}\left(\frac{1}{2}Q_{tot} + Q_d\right) \quad (2)$$

$$Q_d = -qN_dW_d = -\sqrt{2\varepsilon_{ZnO}qN_d\varphi_s} \quad (3)$$

where ζ_{eff} is the effective gate electric field, ε_{ZnO} is the ZnO permittivity (8.66),[35] Q_{tot} ($= C_g|V_G - V_{th}|$) is the total charge density in the ZnO channel, Q_d is the depletion charge density in the ZnO channel, N_d is the doping density, W_d is the depletion region width, and φ_s is the surface barrier potential. The effective gate electric field, ζ_{eff}, can be considered in terms of the initial field (ζ_0) before proton irradiation, the local electric field (ζ_{loc}), and the surface depletion electric field (ζ_{dep}) after irradiation. For the convenience of our discussion, we assume that ζ_{dep} before and after a short irradiation time is much weaker than that after a long irradiation time. Therefore, ζ_{eff} can be expressed as a combination of ζ_0 and ζ_{loc} in the case of a short irradiation time,

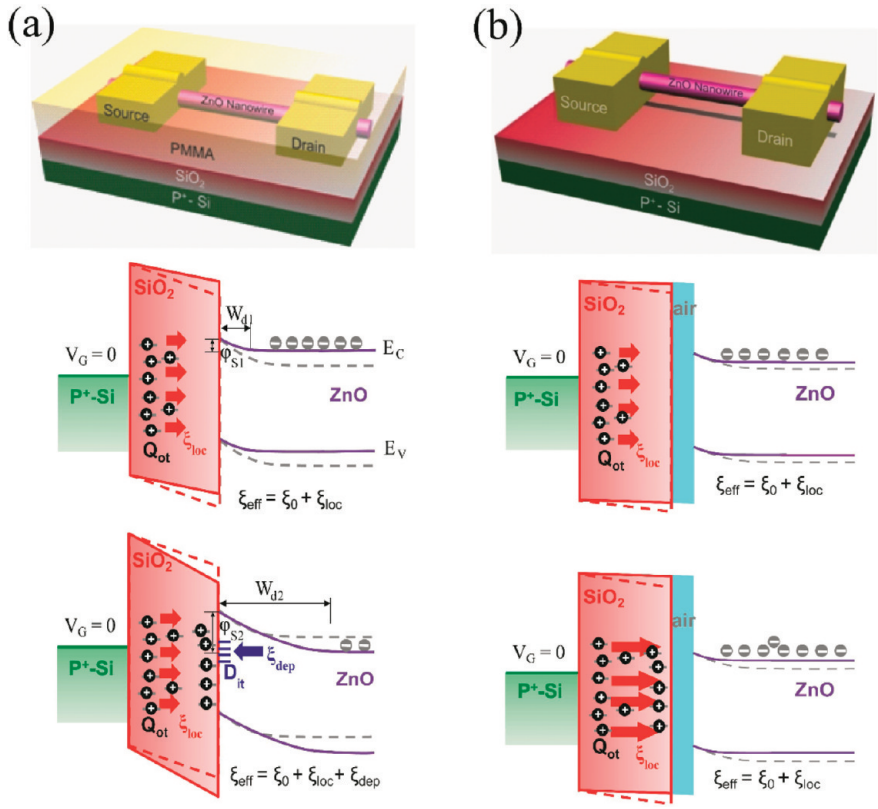

Figure 5. Schematic views and energy band diagrams of (a) the on-substrate-type and (b) the suspended-type ZnO nanowire FETs before and after a short irradiation time (middle) and a long irradiation time (bottom). The red and blue arrows indicate the electric field modulation due to proton irradiation-induced charges (see text for details).

whereas in the case of a long irradiation time, ζ_{eff} is expressed as a combination of ζ_0, ζ_{loc}, and ζ_{dep}. Consequently, the electrical characteristics of the on-substrate-type transistors after a short irradiation time exhibit a negative threshold voltage shift and an electrical conductance increase due to the relatively higher effective gate electric field ($\zeta_{eff,before} = \zeta_0 < \zeta_{eff,after} = \zeta_0 + \zeta_{loc}$) under the same gate bias, whereas those after a long irradiation time exhibit a positive shift and a conductance decrease due to the lower effective gate electric field ($\zeta_{eff,before} = \zeta_0 > \zeta_{eff,after} = \zeta_0 + \zeta_{loc} + \zeta_{dep}$). This proton irradiation effects are clearly observed and shown in Figures 1 and 2, and in Figure S3 in the Supporting Information.

On the other hand, for the case of the suspended-type devices, there is no ζ_{dep} due to the absence of irradiation-induced interface states. Thus, although the gating effect of the suspended-type devices is weaker than that of the on-substrate-type devices, ζ_{eff} is always higher than that before irradiation ($\zeta_{eff,before} < \zeta_{eff,after} = \zeta_0 + \zeta_{loc}$). Consequently, the electrical characteristics of the suspended-type transistors can exhibit an electrical conductance increase after both short and long irradiation times (see Figure 3 and Figure S4 in the Supporting Information).

SUMMARY AND CONCLUSION

Two types (on-substrate and suspended) of ZnO nanowire FET devices were fabricated and systematically characterized before and after the proton irradiation. The electrical characteristics of the on-substrate-type FETs demonstrated that the threshold voltage shift and electrical conductance can be modulated controllably by proton-irradiation-induced charges. The electrical characteristics of the suspended-type devices and PL studies provided substantial evidence that the threshold voltage shift and the electrical conductance modulation are due to the gate electric field modulation, resulting from the combination effects of irradiation-induced positive oxide traps and negative interface traps. Our study enhances the understanding of the proton irradiation effect on nanoscale devices and also provides a potentially useful way to create property-tailored nanoscale devices for developing practical electronic devices.

EXPERIMENTAL METHODS

Two types of FET devices, that is, on-substrate-type devices where nanowires are placed on the substrate and suspended-type devices where nanowires are suspended above the substrate, were fabricated using single-crystal ZnO nanowires. The general growth method of ZnO nanowires by vapor transport and the fabrication method of on-substrate-type nanowire FETs have been described in detail elsewhere.[35] All the fabricated on-substrate-type FET devices were passivated by PMMA to minimize the influence of water or gas molecules on ZnO nanowire FETs and to improve the FET performance by enhancing the gate-coupling effects.[26,35] The suspended-type FETs were fabricated in the following way. First, a thin photoresistor (PR) layer was coated on a silicon substrate with 300 nm-thick SiO_2 using spin-coating at 8000−10000 rpm, followed by soft-baking. Then the suspension of ZnO nanowires was dropped onto the thin PR-coated substrates. A second thick PR layer was coated on the ZnO nanowire-dropped substrates by spin-coating at 4000 rpm, followed by soft-baking in an oven at 90−100 °C for 10 min. Finally, metal electrodes consisting of Ti (200 nm)/Au (200 nm) were defined as source and drain electrodes using the standard photolithography and lift-off process. More details of the fabrication process of the suspended-type FET devices are shown in Figure 3a.

For the proton irradiation experiments, accelerated proton beams were generated using a MC-50 cyclotron (at the Korea Institute of Radiological and Medical Sciences). In our study, the proton beam energy was 10 MeV and the total fluences (Φ) during proton irradiation were 10^{10}, 10^{11}, and 10^{12} cm^{-2}. The proton beam used in our study had a uniformity of about 90% or better, its average beam current was 10 nA, and its irradiated area was 5 × 5 cm^2. The electrical properties of both the on-

substrate-type and suspended-type FETs were characterized systematically before and after proton irradiation using a semiconductor parameter analyzer (HP4155C) at room temperature. Microphotoluminescence (μPL) and temperature-dependent PL studies with a 325 nm He−Cd laser as an excitation source were carried out to investigate the optical properties of the ZnO nanowires before and after proton irradiation.

Acknowledgment. This work was supported in part by the Proton Accelerator User Program, the National Research Laboratory (NRL) Program, the National Core Research Center grant, and the World Class University (WCU) program from the Korean Ministry of Education, Science and Technology (MEST), and the Program for Integrated Molecular System at GIST. J.I.S. and M.E.W. were supported by the European Union through the FP7 Project Nabab (Contract FP7-216777).

Supporting Information Available: $I_{DS}-V_G$ hysteresis curves of on-substrate type ZnO nanowire FET devices. Electrical characteristics of on-substrate type and suspended type ZnO nanowire FET devices before and after proton irradiation with the fluence of $\Phi = 10^{11}$ cm^{-2}. This material is available free of charge *via* the Internet at http://pubs.acs.org.

REFERENCES AND NOTES

1. Kolmakov, A.; Klenov, D. O.; Lilach, Y.; Stemmer, S.; Moskovits, M. Enhanced Gas Sensing by Individual SnO_2 Nanowires and Nanobelts Functionalized with Pd Catalyst Particles. *Nano Lett.* **2005**, *5*, 667–673.
2. Liao, L.; Fan, H. J.; Yan, B.; Zhang, Z.; Chen, L. L.; Li, B. S.; Xing, G. Z.; Shen, Z. X.; Wu, T.; Sun, X. W.; *et al*. Ferroelectric Transistors with Nanowire Channel: Toward Nonvolitile Memory Applications. *ACS Nano* **2009**, *3*, 700.
3. Lai, Q.; Zhang, L.; Li, X.; Stickle, W. F.; Zhu, Z.; Gu, Z.; Kamins, T. I.; Williams, R. S.; Chen, Y. An Organic/Si Nanowire Hybrid Field Configurable Transistor. *Nano Lett.* **2008**, *8*, 876–880.
4. Cui, Y.; Lieber, C. M. Functional Nanoscale Electronic Devices Assembled Using Silicon Nanowire Building Blocks. *Science* **2001**, *291*, 851–853.
5. Lin, M. C.; Chu, C. J.; Tsai, L. C.; Lin, H. Y.; Wu, C. S.; Wu, Y. P.; Wu, Y. N.; Shieh, D. B.; Su, Y. W.; Chen, C. D. Control and Detection of Organosilane Polarization on Nanowire Field-Effect Transistors. *Nano Lett.* **2007**, *7*, 3656–3661.
6. Park, I.; Li, Z.; Pisano, A. P.; Williams, R. S. Selective Surface Functionalization of Silicon Nanowires *via* Nanoscale Joule Heating. *Nano Lett.* **2007**, *7*, 3106–3111.
7. Xiang, J.; Lu, W.; Hu, Y.; Wu, Y.; Yan, H.; Lieber, C. M. Ge/Si Nanowire Heterostructures as High-Performance Field-Effect Transistors. *Nature* **2006**, *441*, 489–493.
8. Lauhon, L. J.; Gudikson, M. S.; Wang, D.; Lieber, C. M. Epitaxial Core−Shell and Core−Multishell Nanowire Heterostructures. *Nature* **2002**, *420*, 57–61.
9. Akamatsu, K.; Tsuruoka, T.; Nawafune, H. Band Gap Engineering of CdTe Nanocrystals through Chemical Surface Modification. *J. Am. Chem. Soc.* **2005**, *127*, 1634–1635.
10. Lin, Y.-M.; Appenzeller, J.; Avouris, P. Ambipolar-to-Unipolar Conversion of Carbon Nanotube Transistors by Gate Structure Engineering. *Nano Lett.* **2004**, *4*, 947–950.
11. Ma, R.-M.; Dai, L.; Huo, H.-B.; Xu, W.-J.; Qin, G. G. High-Performance Logic Circuits Constructed on Single CdS Nanowires. *Nano Lett.* **2007**, *7*, 3300–3304.
12. Zhang, Z.; Liang, X.; Wang, S.; Yao, K.; Hu, Y.; Zhu, Y.; Chen, Q.; Zhou, W.; Li, Y.; Yao, Y.; Zhang, J.; Peng, L.-M. Doping-Free Fabrication of Carbon Nanotube Based Ballistic CMOS Devices and Circuits. *Nano Lett.* **2007**, *7*, 3603–3607.
13. Zheng, Y.; Ni, G.-X.; Toh, C.-T.; Zeng, M.-G.; Chen, S.-T.; Yao, K.; Özilmaz, B. Gate-Controlled Nonvolatile Graphene-Ferroelectric Memory. *Appl. Phys. Lett.* **2009**, *94*, 163505.
14. Paruch, P.; Posadas, A.-B.; Dawber, M.; Ahn, C. H.; McEuen, P. L. Polarization Switching Using Single-Walled Carbon Nanotubes Grown on Epitaxial Ferroelectric Thin Films. *Appl. Phys. Lett.* **2008**, *93*, 132901.
15. Ho, J. C.; Yerushalmi, R.; Jacobson, Z. A.; Fan, Z; Alley, R. L.; Javey, A. Controlled Nanoscale Doping of Semiconductors *via* Molecular Monolayers. *Nat. Mater.* **2008**, *7*, 62–67.
16. Park, G. -S.; Lee, E. K.; Lee, J. H.; Park, J.; Kim, S. K.; Li, X. S.; Park, J. C.; Chung, J. G.; Jeon, W. S.; Heo, S.; *et al*. A High-Density Array of Size-Controlled Silicon Nanodots in a Silicon Oxide Nanowire by Electron-Stimulated Oxygen Expulsion. *Nano Lett.* **2009**, *9*, 1780–1786.
17. Teweldebrhan, D.; Balandin, A. A. Modification of Graphene Properties due to Electron-Beam Irradiation. *Appl. Phys. Lett.* **2009**, *94*, 013101.
18. Krasheninnikov, A. V.; Banhart, F. Engineering of Nanostructured Carbon Materials with Electron or Ion Beams. *Nat. Mater.* **2007**, *6*, 723–733.
19. Gómez-Navarro, C.; De Pablo, P. J.; Gómez-Herrero, J.; Biel, B.; Garcia-Vidal, F. J.; Rubio, A.; Flores, F. Tuning the Conductance of Single-Walled Carbon Nanotubes by Ion Irradiation in the Anderson Localization Regime. *Nat. Mater.* **2005**, *4*, 534–539.
20. Banhart, F. Irradiation Effects in Carbon Nanostructures. *Rep. Prog. Phys.* **1999**, *62*, 1181–1221.
21. Marquardt, C.; Dehm, S.; Vijayaraghavan, A.; Blatt, S.; Hennrich, F.; Krupke, R. Reversible Metal-Insulator Transitions in Metallic Single-Walled Carbon Nanotubes. *Nano Lett.* **2008**, *8*, 2767–2772.
22. Vijayaraghavan, A.; Kanzaki, K.; Suzuki, S.; Kobayashi, Y.; Inokawa, H.; Ono, Y.; Kar, S.; Ajayan, P. M. Metal-Semiconductor Transition in Single-Walled Carbon Nanotubes Induced by Low-Energy Electron Irradiation. *Nano Lett.* **2005**, *5*, 1575–1579.
23. Jo, G.; Hong, W.-K.; Sohn, J. I.; Jo, M.; Shin, J.; Welland, M. E.; Hwang, H.; Geckeler, K. E.; Lee, T. Hybrid Complementary Logic Circuits of One-Dimensional Nanomaterials with Adjustment of Operation Voltage. *Adv. Mater.* **2009**, *21*, 2156–2160.
24. Zhang, Z.; Wang, S.; Ding, L.; Liang, X.; Pei, T.; Shen, J.; Xu, H.; Chen, Q.; Cui, R.; Li, Y.; Peng, L.-M. Self-Aligned Ballistic n-Type Single-Walled Carbon Nanotube Field-Effect Transistors with Adjustable Threshold Voltage. *Nano Lett.* **2008**, *8*, 3696–3701.
25. Yeom, D.; Keem, K.; Kang, J.; Jeong, D.-Y.; Yoon, C.; Kim, D.; Kim, S. NOT and NAND Logic Circuits Composed of Top-Gate ZnO Nanowire Field-Effect Transistors with High-*k* Al_2O_3 Gate Layers. *Nanotechnology* **2008**, *19*, 265202.
26. Kim, W.; Javey, A.; Vermesh, O.; Wang, Q.; Li, Y.; Dai, H. Hysteresis Caused by Water Molecules in Carbon Nanotube Field-Effect Transistors. *Nano Lett.* **2003**, *3*, 193.
27. Sze. S. *Physics of Semiconductor Devices*, 2nd ed.; Wiley: New York, 1981; pp 314−324.
28. Taur, Y.; Ning, T. H. *Fundamentals of Modern VLSI Devices*; Cambridge University Press: Cambridge, U.K., 1998; pp 117−125.
29. Schwank, J. R.; Shaneyfelt, M. R.; Fleetwood, D. M.; Felix, J. A.; Dodd, P. E.; Paillet, P.; Ferlet-Cavrois, V. Radiation Effects in MOS Oxides. *IEEE Trans. Nucl. Sci.* **2008**, *55*, 1833–1853.
30. Oldham, T. R.; McLean, F. B. Total Ionizing Dose Effects in MOS Oxides and Devices. *IEEE Trans. Nucl. Sci.* **2003**, *50*, 483–499.
31. Ma, T. P.; Dressendorfer, P. V. *Ionizing Radiation Effects in MOS Devices and Circuits*; Wiley: New York, 1989.
32. Hu, Y.; Liu, Y.; Li, W.; Gao, M.; Liang, X.; Li, Q.; Peng, L. -M. Observation of a 2D Electron Gas and the Tuning of the Electrical Conductance of ZnO Nanowires by Controllable Surface Band-Bending. *Adv. Funct. Mater* **2008**, *19*, 2390–2387.
33. The carrier density, $n_e = Q_{tot}/(e\pi r^2 L)$, can be determined from the total charge, $Q_{tot} = C_g|V_G - V_{th}|$ in the nanowire, where C_g is the gate oxide capacitance and V_{th} is the threshold voltage required to deplete the nanowire. The C_g can be estimated using a model of a cylinder on an infinite metal plate, $C_g = 2\pi\varepsilon_r/\cosh^{-1}(1 + h/r)$, where r is the nanowire radius, L is the nanowire channel length, h is the SiO_2 thickness, ε_r is the relative dielectric constant of SiO_2.

34. Zhang, Z.; Yao, K.; Liu, Y.; Jin, C.; Liang, X.; Chen, Q.; Peng, L.-M. Quantitative Analysis of Current−Voltage Characteristics of Semiconducting Nanowires: Decoupling of Contact Effects. *Adv. Funct. Mater.* **2007**, *17*, 2478–2489.
35. Hong, W.-K.; Sohn, J. I.; Hwang, D.-K.; Kwon, S.-S.; Jo, G.; Song, S.; Kim, S.-M.; Ko, H.-J.; Park, S.-J.; Welland, M. E.; Lee, T. Tunable Electronic Transport Characteristics of Surface-Architecture-Controlled ZnO Nanowire Field Effect Transistors. *Nano Lett.* **2008**, *8*, 950.
36. Burlacu, A.; Ursaki, V. V.; Skuratov, V. A.; Lincot, D.; Pauporte, T.; Elbelghiti, H.; Rusu, E. V.; Tiginyanu, I. M. The Impact of Morphology upon the Radiation Hardness of ZnO Layers. *Nanotechnology* **2008**, *19*, 215714.
37. Coskun, C.; Look, D. C.; Farlow, G. C.; Sizelove, J. R. Radiation Hardness of ZnO at Low Temperatures. *Semicond. Sci. Technol.* **2004**, *19*, 752–754.
38. Özgür, Ü.; Alivov, Ya. I.; Liu, C.; Teke, A.; Reshchikov, M. A.; Doğan, S.; Avrutin, V.; Cho, S.-J.; Morkoç, H. A Comprehensive Review of ZnO Materials and Devices. *J. Appl. Phys.* **2005**, *98*, 041301.
39. Look, D. C.; Reynolds, D. C.; Hemsky, J. W.; Jones, R. L.; Sizelove, J. R. Production and Annealing of Electron Irradiation Damage in ZnO. *Appl. Phys. Lett.* **1999**, *75*, 811.
40. Djurišić, A. B.; Leung, Y. H. Optical Properties of ZnO Nanostructures. *Small* **2006**, *2*, 944.
41. Reynolds, D. C.; Look, D. C.; Jogai, B. Fine Structure on the Green Band in ZnO. *J. Appl. Phys.* **2001**, *89*, 6189–6191.
42. Hong, W.-K.; Jo, G.; Choe, M.; Lee, T.; Sohn, J. I.; Welland, M. E. Influence of Surface Structure on the Phonon-Assisted Emission Process in the ZnO Nanowires Grown on Homoepitaxial ZnO Films. *Appl. Phys. Lett.* **2009**, *94*, 043103.
43. Mandal, S.; Sambasivarao, K.; Dhar, A.; Ray, S. K. Photoluminescence and Electrical Transport Characteristics of ZnO Nanorods Grown by Vapor-Solid Technique. *J. Appl. Phys.* **2009**, *106*, 024103.
44. Calarco, R.; Marso, M.; Richter, T.; Aykanat, A. I.; Meijers, R.; v. d. Hart, A.; Stoica, T.; Lüth, H. Size-Dependent Photoconductivity in MBE-Grown GaN-Nanowires. *Nano Lett.* **2005**, *5*, 981–984.
45. Cavallini, A.; Polenta, L.; Rossi, M. Franz−Keldysh Effect in GaN Nanowires. *Nano Lett.* **2007**, *7*, 2166–2170.